AD-A133 975 ELECTROSTATIC ION-CYCLOTRON WAVES IN MAGNETOSPHERIC PLASMAS: NON-LOCAL ASPECTS(U) NAVAL RESEARCH LAB WASHINGTON DC G GANGULI ET AL. 14 OCT 83 NRL-MR-5197 1/1

UNCLASSIFIED F/G 20/9 NL

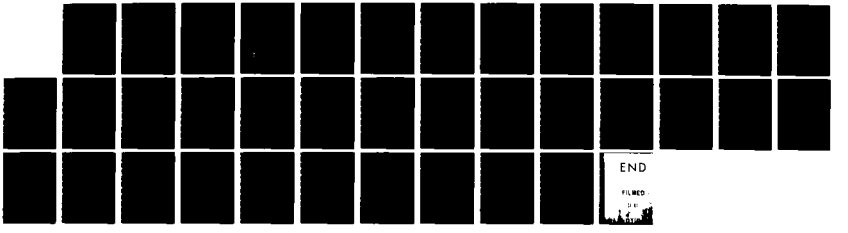

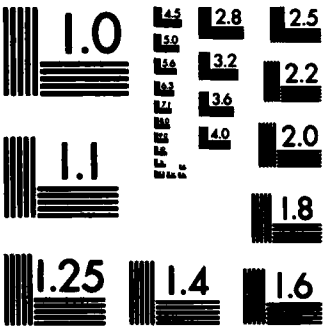

MICROCOPY RESOLUTION TEST CHART
NATIONAL BUREAU OF STANDARDS-1963-A

(2)

AD-A133 975

NRL Memorandum Report 5197

Electrostatic Ion-Cyclotron Waves in Magnetospheric Plasmas: Non-Local Aspects

G. GANGULI,* P. BAKSHI,* AND P. PALMADESSO

Geophysical and Plasma Dynamics Branch
Plasma Physics Division

**Science Applications, Inc.*
McLean, VA 22102

October 14, 1983

This research was sponsored by the Office of Naval Research and the National Aeronautics and Space Administration.

NAVAL RESEARCH LABORATORY
Washington, D.C.

SECURITY CLASSIFICATION OF THIS PAGE (When Data Entered)

REPORT DOCUMENTATION PAGE		READ INSTRUCTIONS BEFORE COMPLETING FORM
1. REPORT NUMBER NRL Memorandum Report 5197	2. GOVT ACCESSION NO. AD-A133 975	3. RECIPIENT'S CATALOG NUMBER
4. TITLE (and Subtitle) ELECTROSTATIC ION-CYCLOTRON WAVES IN MAGNETOSPHERIC PLASMAS: NON-LOCAL ASPECTS		5. TYPE OF REPORT & PERIOD COVERED Interim report on a continuing NRL problem. 6. PERFORMING ORG. REPORT NUMBER
7. AUTHOR(s) G. Ganguli,* P. Bakshi,* and P. Palmadesso		8. CONTRACT OR GRANT NUMBER(s)
9. PERFORMING ORGANIZATION NAME AND ADDRESS Naval Research Laboratory Washington, DC 20375		10. PROGRAM ELEMENT, PROJECT, TASK AREA & WORK UNIT NUMBERS 61153N; RR033-02-44; W-14365; 47-0884-0-3; 47-1447-0-3
11. CONTROLLING OFFICE NAME AND ADDRESS Office of Naval Research Arlington, VA 22203 NASA Washington, DC 20546		12. REPORT DATE October 14, 1983 13. NUMBER OF PAGES 36
14. MONITORING AGENCY NAME & ADDRESS(if different from Controlling Office)		15. SECURITY CLASS. (of this report) UNCLASSIFIED 15a. DECLASSIFICATION/DOWNGRADING SCHEDULE

16. DISTRIBUTION STATEMENT (of this Report)

Approved for public release; distribution unlimited.

17. DISTRIBUTION STATEMENT (of the abstract entered in Block 20, if different from Report)

18. SUPPLEMENTARY NOTES

*Present address: Science Applications, Inc., McLean, VA 22102
P. Bakshi - permanent address: Department of Physics, Boston College, Chestnut Hill, MA 02167
This research was sponsored by the Office of Naval Research and the National Aeronautics and Space Administration.

19. KEY WORDS (Continue on reverse side if necessary and identify by block number)

EIC waves
Non-local effects
Magnetospheric plasma

20. ABSTRACT (Continue on reverse side if necessary and identify by block number)

The importance of the effect of the magnetic shear and the finite size of the current channel on the electrostatic ion-cyclotron instability for the space plasmas is illustrated. A non-local treatment is used. When the channel width L_c, is larger than the shear length L_s, there is a large reduction in the growth rate along with a noteworthy reduction of the band of the unstable perpendicular wavelengths. For $L_c \leq L_s/10$ the growth rate is not much altered from its local value; however for $L_c/\rho_i \leq 10^2$ the growth rate starts falling below the local value and vanishes for $L_c \sim \rho_i$. The non-local effects lead to enhanced coherence in the ion cyclotron waves.

DD FORM 1 JAN 73 1473 EDITION OF 1 NOV 65 IS OBSOLETE
S/N 0102-014-6601

SECURITY CLASSIFICATION OF THIS PAGE (When Data Entered)

CONTENTS

ELECTROSTATIC ION-CYCLOTRON WAVES IN MAGNETOSPHERIC PLASMAS: NON-LOCAL ASPECTS

I. INTRODUCTION

The current driven ion-cyclotron instability (CDICI) has been of considerable interest to space plasma physicists. Recent observations by Kintner (1980) and Kintner et al. (1978) have made it very topical. Drummond and Rosenbluth (1962) were first to examine this instability analytically while Kindel and Kennel (1971) studied it in the context of space plasmas in the earth's magnetosphere. The results from Kindel and Kennel have frequently been applied to observations involving the electrostatic CDICI in space. It should be noted, however, that the analysis of both Drummond and Rosenbluth and Kindel and Kennel is a local analysis. They consider a uniform zeroth order magnetic field (i.e., $\underline{B} = B_0\hat{z}$), thereby neglecting the self-consistent magnetic field generated by the field aligned currents. This magnetic field (usually small) will give rise to a shear in the zero order magnetic field (see Figure 1) and consequently make the zero order field space dependent (i.e., $\underline{B}(x) = B_y(x)\hat{y} + B_z\hat{z}$, where shear is in the x-direction).

In general, magnetic shear is a damping agent and can significantly alter the local mode structure (e.g., it was shown by Ross and Mahajan, (1978) that an infinitesimal shear can completely damp the universal drift instability). Recently Waltz and Dominguez (1981), motivated by the TFR (1978) tokamak experiment, have provided numerical results for the behavior of CDICI in a sheared magnetic field pertinent to the TFR (1978) parameters. Ganguli and Bakshi (1982) have given a detailed analytical treatment of the CDICI in a sheared magnetic field and have concluded that even a small shear can give a significant reduction in the growth rates. It also greatly reduces the region of unstable perpendicular wavelengths.

The above mentioned treatments of shear implicitly assume that a uniform shear prevails over a large enough region of space. A finite current channel size, of width L_c, may introduce important modifications when L_c becomes comparable to or smaller than the shear length L_s. Recently Bakshi, Ganguli and Palmadesso (1983) have developed the theory for the effects of shear on CDICI, taking into consideration the role played by a finite width current channel. The main result of that

Manuscript approved August 9, 1983.

investigation shows that the growth rate is given by the pure shear theory when $L_c > L_s$ and reverts to the local growth rate if $L_c << L_s$, with a smooth transition as a function of (L_c/L_s). There is another non-local effect, due to the variation of the current profile across the slab, which leads to quenching of the instability if the slab width is reduced to only a few ion gyro radii.

In this paper we illustrate the importance of these non-local treatments of the CDICI for the space plasmas. We show that the non-local theory can, under certain circumstances, lead to enhanced coherence in the electrostatic CDICI.

II. THEORY

a. Assumptions

We consider a slab geometry where both the electrons and the ions have a Gaussian distribution function. The plasma has a negligible β ($\beta \equiv \frac{8\pi nkT}{B^2} << 1$), and the electrons drift with respect to the ions along the magnetic field with a velocity V_d. Both species have a finite non-zero temperature $T_\alpha = m_\alpha v_\alpha^2/2\, k_B$, α denoting the species, m_α is the mass, v_α is the thermal velocity and k_B is the Boltzmann's constant. We neglect the term $(k\lambda_\alpha)^2 << 1$ where k is the wavevector in arbitrary direction while λ_α is the Debye length. Since for most space plasmas of interest, the ion and electron temperatures are of the same order, we shall restrict the analysis here for the temperature ratio $\tau \equiv T_i/T_e = O(1)$. The ambient magnetic field is in the $\hat{y}$-$\hat{z}$ plane and contains a shear in the $\hat{x}$-direction. Let us first consider a simple model for a sheared magnetic field, given by

$$\underline{B} = B_o\{\hat{z} + (x/L_s)\hat{y}\}, \tag{1}$$

with $x/L_s << 1$ and $L_s = (\partial\theta/\partial x)^{-1}$ where $\theta = \tan^{-1}(B_y/B_z)$. Thus L_s is the scale length characterizing the magnetic shear. In the absence of shear the field configuration is $\underline{B} = B_o\hat{z}$.

In a shear free field the plasma is unstable to the CDICI when $\omega - k_\parallel V_d < 0$ for ω and $k_\parallel$ consistent with the dispersion relation. The waves at maximum growth (for $T_e \approx T_i$) are characterized by $\omega_r \sim \Omega_i$, $\Omega_i = eB_o/m_i c$, the ion Larmour frequency; $\gamma \ll \omega_r$; and $k\rho_i \approx 0(1)$ where $\rho_i = (2k_B T_i/m_i)^{1/2}/\Omega_i$, is the ion Larmour radius. Electron Landau and ion-cyclotron damping reduce the growth rate depending on the magnitude of $k_\parallel$ (see Ganguli and Bakshi (1982)).

The above description of the plasma gets significantly modified by the introduction of a shear in the magnetic field as given in expression (1). The magnetic field rotates in the $\hat{y}$-$\hat{z}$ plane (see Figure 1) as a function of x. If at $x = 0$ we have $k_\parallel = 0$ then at $x = x_1$ we see that $k_\parallel \neq 0$ since at x_1 the magnetic field has rotated by an angle $\theta_1 = x_1/L_s$. Thus the dispersive properties of the plasma are also a function of x. It is this effect which changes the boundary condition from plane waves to outgoing energy flux condition and which the local theory fails to account for, thereby giving incomplete results.

We introduce shear (i) locally, by replacing $k_\parallel$ by $k_\parallel^o + sk_y x$, where $s = 1/L_s$ and (ii) globally by replacing ik_x by "$\frac{\partial}{\partial x}$". Since the magnitude of the magnetic shear of interest to us is quite small, we neglect the orbital effects of shear [Bakshi, Bellew, Ganguli and Satyanarayana (1977), Bellew (1978), Ganguli (1980) and Linsker (1981)] arising mainly out of the shear kinematic drift of the particles in the sheared magnetic field.

b. Dispersion Relation

The general dispersion relation for CDICI in the absence of shear is given by

$$k^2 + \sum_{n,\alpha} \frac{\Gamma_n(b_\alpha)}{\lambda_\alpha^2} \left[1 + \left(\frac{\omega - k_\parallel V_{d\alpha}}{|k_\parallel| v_\alpha}\right) Z \left(\frac{\omega - n\Omega_\alpha - k_\parallel V_{d\alpha}}{|k_\parallel| v_\alpha}\right)\right] = 0, \qquad (2)$$

where $b_\alpha = k_\perp^2 \rho_\alpha^2/2$, $\Gamma_n(b) = I_n(b)e^{-b}$ and $I_n(b)$ are modified Bessel's function.

As previously described we study the effects of the magnetic shear by replacing $k_\parallel$ by $k_y u$, where $u = sx(\equiv k_\parallel(x)/k_y)$ and ik_x by $\frac{\partial}{\partial x}$ in equation (2) (we have assumed $k_\parallel^o = 0$). Transforming to the ion frame (i.e., setting $V_{di} = 0$), retaining the $n = 0$ term for the electrons and $n = 0, \pm 1, \pm 2$

terms for the ions (since we wish to study the first harmonic only) and expanding $\Gamma_n(b-(\rho_i^2/2)\partial^2/\partial x^2)$ to $O(\partial^2/\partial x^2)$ (here $b = k_y^2\rho_i^2/2$), we obtain a second order differential equation for the electrostatic potential $\phi(x)$,

$$\{-A(x)\frac{\partial^2}{\partial x^2} + Q_1(x)\}\phi(x) = 0. \tag{3}$$

The equation can be reduced to (see Ganguli and Bakshi (1982)),

$$\{(\rho_i s)^2\frac{\partial^2}{\partial u^2} + Q(u)\}\phi(u) = 0, \tag{4}$$

where,

$$Q(u) = -\frac{Q_1(u)}{\hat{A}(u)},$$

$$Q_1(u) = 1 + \tau + \zeta_i\Gamma_o Z(\zeta_i) + \zeta_i\Gamma_1\{Z((i-p)\zeta_i) + Z((1+p)\zeta_i)\}$$

$$+ \zeta_i\Gamma_2\{Z((1-2p)\zeta_i) + Z((1+2p)\zeta_i)\}$$

$$+ \tau\zeta_e(1 - \frac{k_\parallel V_d}{\omega})Z(\zeta_e(1-\frac{k_\parallel V_d}{\omega})),$$

$$\hat{A}(u) = (\frac{\zeta_i}{2})[Z(\zeta_i)\Gamma_o' + \{Z((1-p)\zeta_i)) + Z((1+p)\zeta_i)\}\Gamma_1'$$

$$+ \{Z((1-2p)\zeta_i) + Z((1+2p)\zeta_i)\}\Gamma_2'],$$

and

$$\Gamma_n' = \frac{\partial\Gamma_n}{\partial b}.$$

We have assumed $k_x^2 << k_y^2$ in neglecting higher order derivatives in the expansion of Γ_n.

As shown in Ganguli and Bakshi (1982) we expand the "potential", Q(u) of the differential equation (4) around $\xi = (u-u_o) = 0$ to $O(\xi^2)$. Here u_o is the angle of propagation for the maximum growth rate in the absence of shear. We thus obtain,

$$\{(\rho_i s)^2\frac{\partial^2}{\partial\eta^2} + a + \frac{Q_o''}{2}\eta^2\}\phi(\eta) = 0, \tag{5}$$

where,

$$\eta = \xi + Q_o'/Q_o'',$$

$$a = Q_o - Q_o'^{\,2}/2Q_o'',$$

and

$$Q_o = Q(u_o),\ Q_o' = \frac{d}{du}\ Q(u)\big|_{u=u_o},\ Q_o'' = \frac{d^2}{du^2}\ Q(u)\big|_{u=u_o}.$$

The dispersion relation under the outgoing energy flux boundary condition similar to Pearlstein and Berk (1969), is

$$Q(\omega,u_o) = (2\ \ell+1)(\rho_i s)(-Q_o''/2)^{1/2} + Q_o'^{\,2}/2Q_o''. \qquad (6)$$

Note $Q(\omega,u_o) = 0$ yields the local dispersion relation maximized over $k_\parallel$, while the right hand side of the equation (6) arises from of the non-local treatment. The first term in the right hand side is proportional to the magnetic shear and vanishes in the zero shear limit. The second term, is not explicitly shear dependent. This term can contribute significantly even for infinitesimal shear thereby making the non-local dispersion relation solutions much different from those of the local dispersion relation.

c. Finite Slab Effects.

We have given elsewhere (Bakshi, Ganguli and Palmadesso, 1983) the details of the modifications brought about by the finite slab size L_c. A finite width current is introduced by taking the electron distribution function to be a shifted Maxwellian with a drift velocity parallel to the magnetic field given by

$$V_d(x) = V_d^o\ g(x_g/L_c),$$

$$g(\xi) = e^{-\xi^2},\ x_g = x + \frac{V_y}{\Omega_e}. \qquad (7)$$

If we ignore the very small effects of order ρ_e^2/L_c^2, where ρ_e is the electron gyro-radius, the current profile is found to be

$$j(x) = n_o e V_d^o g(\xi), \quad \xi \equiv \frac{x}{L_c} . \tag{8}$$

Such a current profile generates a self-consistent shear in the magnetic field, given by

$$\frac{B_y(x)}{B_z} = \frac{L_c}{L_s} \int_o^\xi g(\xi) d\xi, \tag{9}$$

where the shear length is defined by

$$\frac{1}{s} = L_s = \frac{cB_z}{4\pi n_o e V_d^o} . \tag{10}$$

The corresponding variation in the parallel wavenumber,

$$k_\parallel(x) = k_\parallel^o + k_y B_y(x)/B_z, \tag{11}$$

leads to the variation in the angle of propagation

$$u(x) = \frac{k_\parallel(x)}{k_y} = u_o + \frac{L_c}{L_s} \int_o^\xi g(\xi) d\xi. \tag{12}$$

Thus the relation between the angle u and the physical distance x, or the scaled physical distance ξ is no longer linear. The non-local effects are again described by the differential equation obtained by letting $k_x \to (1/i)d/dx$, and $k_\parallel \to k_\parallel(x)$ as given by eq. (11) and $V_d \to V_d(x)$ as implied by eq. (8),

$$\left[\rho_i^2 \frac{d^2}{dx^2} + Q(u(x), V_d(x))\right]\phi = 0 \tag{13a}$$

or

$$\left[\left(\frac{\rho_i}{L_c}\right)^2 \frac{d^2}{d\xi^2} + Q(u, V_d)\right]\phi = 0, \tag{13b}$$

with Q defined as in (4) apart from the x-dependence as stated above. Expanding Q around ξ_1, where

$$Q'(\omega, \xi_1) = 0, \tag{14}$$

provides more accurate results as compared to expansion around ξ_o or u_o as in eq. (5), and the dispersion relation which generalizes eq. (6) is given by

$$Q(\omega,\xi_1) = (2\ell + 1)(\rho_i/L_c)\left[-\frac{1}{2}\, Q''(\omega,\xi_1)\right]^{1/2}. \qquad (15)$$

The eigenfrequency obtained from (15) depends on $k_\parallel^o$, which is as yet undetermined. The dominant mode, for a given k_y, is obtained by maximizing $\gamma = \mathrm{Im}\omega(k_\parallel^o)$ over $k_\parallel^o$.

III. RESULTS

We now discuss the implications of the non-local treatments in the preceding section. The results of the uniform shear model are contained in eq. (6), while the finite slab effects are given by eq. (15). Both these are generalizations of the local dispersion relation $Q(\omega,u_o) = 0$.

The non-local dispersion relation (6) is solved numerically by an iterative technique. We simplify the "potential" by expanding all the ion Z-functions except n=1 for large arguments, retain terms to $O(1/\zeta_i^2)$ and treat A(u) as a constant evaluated at u_o. [For details see Ganguli and Bakshi (1982)].

Figure 2 shows a plot of γ/Ω_i against b for various values of the shear and $\tau = 0.5$, $\mu = 1837$, $V_d/v_e = 0.25$. Note the difference between the local solution and the zero shear limit of the non-local solution. This large reduction in the growth rate is due to the second term in equation (6) arising from the non-local treatment. Figure 2 also shows that the value of b for which maximum growth occurs remains essentially unaltered from the local theory, even when shear is increased. In addition to the expected reduction of the maximum growth rate, the primary effect of increased shear is to narrow the band of unstable perpendicular wavelengths. The uneven spacing of the $\rho_i s = 0$, 0.005 and 0.01 curves shows that non-linearity in the shear parameter (through the implicit dependence of ω on $(\rho_i s)$)already sets in at $\rho_i s = 0.01$.

In Figures 3 and 4 we provide additional γ/Ω_i versus b plots for typical space plasma parameters. In Figure 3 we consider a hydrogen plasma: $\mu = 1837$, $\tau = 0.75$, $V_d/v_e = 0.3$ and $\rho_i s = 10^{-6}$. Note once again the big drop in the local growth rate as well as the significant reduction of the unstable perpendicular wavevector band. Figure 4 illustrates the same features for $\tau = 1$, $V_d/v_e = 0.35$ and the other parameters unchanged. The consequence of the non-local treatment is even more drastic in this case. The non-local treatment leads to a completely damped instability.

The drastic changes due to non-local effects stem from the implicit assumption that the driving current prevails over a sufficiently wide region in the x-direction so that $k_\parallel/k_\perp$ can become arbitrarily large. This condition will not be met in many space plasma situations, and we need the results of the finite slab theory (Bakshi, Ganguli, and Palmadesso, 1983), which led to eq. (15).

Consideration of a finite width current sheet leads to two scale lengths, L_s and L_c, which govern the growth rate. Figure 5 shows the variation in (γ/Ω_i) vs. (L_c/ρ_i) for $\tau = 0.5$, $V_d^o/v_e = 0.28$, $\mu = 1837$ and $b = 0.6$, for three different shear parameters $(\rho_i/L_s) = 10^{-4}$, 10^{-5} and 10^{-6}. In each case the growth rate has the significantly reduced value, characteristic of the uniform shear model, if L_c is taken to be sufficiently large. As the slab width is decreased, the growth rate increases and climbs up to the local value when L_c is sufficiently small. Thus, there is a <u>smooth</u> transition from the pure shear reduced γ to the usual local γ.

The three curves in Figure 5 appear very similar, except for a relative displacement, and the essential universality of the transition curve (for small shears) can be brought out by plotting γ vs. (L_c/L_s) as in Figure 6. The shear reduced γ prevails for $L_c \gtrsim L_s$, and the three curves continue to overlap for $L_c > (L_s/20)$. The curve describing the weakest shear $\rho_i/L_s = 10^{-6}$ almost attains the local value when $L_c \approx 10^{-2}\ L_s$. The physical reason for this transition to the local value is easily seen: the detuning or misalignment of the magnetic field lines across the length of the slab of order L_c here happens to be too small to have any impact on the instability. On the other hand, when $L_c \gtrsim L_s$, enough misalignment occurs to produce local regions where the angle between the fixed wave direction

$\vec{k}$ and the varying $\vec{B}(x)$ is sufficiently different from the optimal value (typically $k_{\parallel}^{o}/k_{\perp} \sim 1/10$) to produce a much lower average growth rate.

An additional non-local effect, directly due to the variable current profile (and not the shear) is also evident in Figures 5 and 6. After attaining the local growth rate, if the slab size is further reduced, the growth rate again becomes smaller than the local value for $L_c/\rho_i < 10^2$. It is clear from Figure 5 that this effect is not sensitive to the value of the shear (at least in the range considered). The physical explanation for this reduction is also easily seen. The spatial variation of the current has a direct effect on the wave packet ϕ. The reduction of the current away from the center of the slab results in a reduced drive and a corresponding reduced γ. If L_c/ρ_i is further reduced to 10 or lower, a significant reduction γ occurs, with eventual quenching.

A typical potential function ϕ is displayed in Figure 7, with $V_d^o/v_e = 0.28$, $\tau = 0.5$, $\mu = 1837$, $b = 0.6$, $L_s/\rho_i = 10^2$ and $L_c/\rho_i = \infty$. The independent variable u is the physical angle $u = x/L_s$, the origin of x is at the position where the field line is perpendicular to the given $\vec{k}$. As shown, $|\phi|$ is significant between 0.06 and 0.12 with a peak around $u_{mo} = 0.09$. This indicates that the wave propagates in the direction given by $k_{\parallel}^{o} \sim (0.09)k_{\perp}$.

Besides the changes in growth rate, the non-local theory also predicts a transition in the angular position of the peak of $|\phi|$, or in the effective angle u_{mo} between the direction normal to the local field line and the direction of the propagating wave. This is displayed in Figure 8, for the same parameters as in Figure 6, over a wide range of (L_c/L_s). Note the transition from $u_{mo} = 0.13$ characteristic of local theory to the reduced $u_{mo} = 0.09$ of the pure shear dominated limit. The non-local effects thus reduce the effective angle $k_{\parallel}^{o}/k_{\perp}$.

Figure 9 shows the variation of γ as a function of wavenumber. The local theory result prevails for weak shear and $L_c/L_s \lesssim 10^{-2}$, the pure shear dominated reduction occurs for $L_c \gtrsim L_s$ with a smooth transition in between. The $L_c = L_s$ curves, except for a slight change of parameters, correspond to the $\rho_i s \approx 0$ and $\rho_i s = 0.01$ curves of Figure 2.

We have also examined the CDICI in an oxygen plasma and note that the current thresholds are generally much lower compared with those of a

hydrogen plasma. The effect of the non-local treatment for a multispecies plasma is an interesting question which is now being investigated and will be reported elsewhere.

IV. DISCUSSION

There are several implications of the non-local effects discussed above. If the shear is small, we have shown that there are three different regimes depending on the scale size of the current channel, L_c:

(1) For $L_c > (L_s/10)$ there occurs, as compared to the results of the local theory, (a) a reduction in the growth rate, (b) a reduction in the bandwidth of $k_\perp$ over which the instability prevails and (c) a reduction in the angle of propagation $u_{mo} = k_\parallel^o/k_\perp$. This is the shear dominant regime.

(2) For $\rho_i \ll L_c \ll L_s$, one recovers the results of the local theory (except for one important aspect, which we discuss later in this section).

(3) For $L_c \gtrsim \rho_i$, again (a) there is a reduction in the growth rate, and (b) a reduction in the bandwidth of $k_\perp$ over which the instability prevails, but (c) there is no reduction in u_{mo}, as compared to the results of the local theory. The instability is quenched for $L_c \lesssim 2\rho_i$.

Thus we have shown that local theory cannot be applied without reservations; one must first scrutinize the scale lengths for the given laboratory experiment, or the space plasma of interest, to ascertain which regime is relevant. In some situations, (e.g., the case $L_s = 10^3\rho_i$ of Figure 6), the conditions for regime (2) cannot be strictly satisfied for any value of L_c, and the results of the local theory are not applicable. This aspect is accentuated as the shear increases.

In space plasmas, typical shear lengths are $L_s \sim$ few hundred km, and $\rho_i/L_s \sim 10^{-6}$. Thus the smaller sized ($\sim$ 1 km) auroral arcs would not qualify for regime (1). The quiet time, broader Birkeland current Region 1/Region 2 systems may be more appropriate for these effects. Also, since the current sheet width increses with altitude, the effects of regime (1) have a better chance of being significant at higher altitudes.

The transition from the shear-affected regime (1) to the local theory results of regime (2) was shown (Figure 6) to depend on L_c/L_s, essentially described by a universal curve independent of shear. The net change in he growth rate and the range of (L_c/L_s) over which the transition takes place will be governed by the physical parameters μ, τ and V_d/v_e, and the perpendicular wavenumber $k_\perp$. Under what conditions can we expect the effects of shear to be significant?

One can assess these trends by plotting the local growth rate as a function of the angle $k_\parallel/k_\perp$. As an illustration, we note that Figure 1 of Ganguli and Bakshi (1982) displays the effect of varying τ. It shows that the angular band over which the instability can occur becomes narrower as τ increases. The transition from regime (1) to regime (2) can be expected to occur when L_c/L_s, which represents the tilt produced by shear, becomes comparable to this angular bandwidth. Thus one can infer that for a given L_c, increasing τ will favor regime (1), making the shear more effective.

We can test this quantitatively by evaluating the growth rate as a function of L_c/L_s for two different values of τ. Figure 1 of Ganguli and Bakshi (1982) was for a fixed $b = 0.5$. Since the perpendicular wavenumber (or equivalently b) is a free parameter, one must maximize the growth rate over b as well. We have carried out these calculations for $V_d/v_e = 0.4$, $\mu = 1837$, $\tau = 0.5$ and 1, and the results are displayed in Figures 10 and 11. The imaginary part of $Q_1 (\equiv Q_{1I})$, eq. (4), is plotted against $u = k_\parallel/k_\perp$ in Figure 10, with $b = 0.6$, $\omega_o = 1.3037$ for $\tau = 0.5$ and $b = 0.9$, $\omega_o = 1.2027$ for $\tau = 1$. The angular width of the domain where Q_{1I} is negative, indicative of instability, is clearly much smaller for $\tau = 1$.

The corresponding results for the growth rate as a function of (L_c/L_s) are displayed in Figure 11. The growth rate for each τ is normalized to the corresponding local growth rate γ_L. Noticeable departure from the local value begins at $(L_c/L_s) = 0.01$ for $\tau = 1$ and at 0.02 for $\tau = 0.5$, and proceeds much faster for the larger τ as L_c/L_s is increased. Thus the effects of shear are more significant for the larger τ, given a fixed current channel width.

Figure 1 of Ganguli and Bakshi (1982) also shows that the angular band width of the domain of instability increases with increasing V_d/v_e. But an increase in V_d also strengthens the shear, thereby increasing L_c/L_s. Near the threshold drift velocity, (where the system is marginally stable), the increase in angular band width proceeds faster than the increase in L_c/L_s; thus an increase in V_d favors a move towards the local regime (2). On the other hand, if V_d is significantly larger than the threshold for marginal stability, the situation is reversed and an increase in V_d favors a move towards the shear dominated regime (1).

So far, we have only discussed the mode near the cyclotron frequency, $\omega \gtrsim \omega_{ci}$. What can we expect for the higher harmonic modes? The definition of Q_l in eq. (4) must first be modified to include higher n terms from the full dispersion relation, eq. (2). We have evaluated Q_l including terms up to $n = \pm 4$ and maximized over b to obtain optimal local growth rates. The results for Q_{lI} vs. u are displayed in Figure 12 for the first three cyclotron harmonics, with real frequencies $\omega_o = 1.1897$, $b = 0.9$; $\omega_o = 2.2237$, $b = 2.4$; $\omega_o = 3.2499$, $b = 4.8$; and physical parameters $\tau = 1$, $\mu = 1837$, $V_d/v_e = 0.65$. The angular band width of the unstable zone ($Q_{lI} < 0$) becomes significantly smaller for higher harmonics. Thus the transition to the shear dominated regime (1) can be expected to occur for the higher harmonics for progressively smaller values of L_c/L_s.

These considerations show that the results of the local theory, regime (2), cannot be used without reservations, and a transition towards regime (1) is helped by increasing τ, considering higher harmonics, and increasing the drift velocities. It is also accentuated by increasing the current channel width, directly by considering wider channels or for the same current sheet, by scaling with altitude. A detailed numerical study of all of these effects over a wide range of parameters is beyond the scope of this work and will be given elsewhere. We anticipate that some of the situations of practical interest in space plasmas will fall in regime (2) while others will favor a move towards regime (1).

There is a subtler effect, implicit in the non-local treatment, which may be more widely relevant. Once any inhomogeneity is introduced in the x-direction, the symmetry in the x-y plane is broken, and one has to distinguish between the propagation along $\hat{y}$ and the propagation (if any)

along $\hat{x}$. The same inhomogeneity precludes the use of Fourier transforms in the x-direction and the plane wave solutions $e^{ik_x x}$ are necessarily replaced by a wave packet, $\phi(x)$, which is localized (e.g., see Fig. 7) in the x-direction. Since the current systems have the structure of a sheet, the short direction becomes the slab direction and the waves propagate along $\hat{y}$ and $\hat{z}$ with wave vector components $(k_y, k_\parallel)$, $k_y >> k_\parallel$.

Now let us consider the implications of this phenomenon concerning satellite measurements of ion cyclotron waves. A moving observer will see a Doppler shifted frequency

$$\omega' = \omega + \underline{k} \cdot \underline{v}_s$$

where $\underline{v}_s$ is the velocity vector of the observer (satellite) and $\underline{k}$ is the wave vector. Since $\underline{k}$ has no component along x (the wave packet is localized), it follows that a satellite moving perpendicular to the current sheet (i.e., along our $\hat{x}$ direction) will not see any Doppler-shift, irrespective of the size of k_y. Such a statement could not be made in the purely local theory, since there would be no essential difference between the two transverse directions $\hat{x}$ and $\hat{y}$, and waves are as likely to be moving in any direction in the x-y plane. In a local theory, a wide range of Doppler shifts would be produced, from $-k_\perp v_s$ to $+k_\perp v_s$, since the maximum value of k_x is $k_\perp$. Some of the observations on S3-3 indicate no or little Doppler shift. While other explanations may be available, this inference from our non-local treatment must also be considered, since an inhomogeneous plasma mandates a non-local treatment. Thus, the extremely high degree of coherence of many of the observations can be understood in a very simple way. This idea can be further tested by analyzing satellite data from an orbit which crosses the current sheet at a significantly different angle.

Various phenomena described above would lead to an enhanced coherence for the observed ion cyclotron waves as seen by a moving observer. When conditions for regime (1) prevail, there is a significant reduction in the band of perpendicular wave numbers for which the instability can occur. This reduces the magnitude of the Doppler shift $\underline{k} \cdot \underline{v}_s$ as compared to the local theory for any direction of the satellite motion. On the other hand,

the directional preference for $\vec{k}_\perp$, required by the inhomogeneity for all regimes, shows that satellites moving perpendicular to the current sheet would see very coherent ion cyclotron waves, with no Doppler shift, irrespective of the size of $\vec{k}_\perp$. A study of all available observational information for various transit angles of the satellite motion could be very instructive.

V. OUTLOOK

In this paper, we have analyzed the implications of a non-local treatment of the CDICI, which is necessitated by the introduction of an inhomogeneous current profile. One cannot yet provide a detailed comparison between theory and observations; that would require additional work on the theoretical side and more detailed data from the observational side. New data from the Dynamic Explorer would be very helpful in this context.

But even without carrying out the additional theoretical studies, or awaiting the new observational data, a number of interesting questions have been raised in this paper, and it would be very helpful to look at all available data from a different angle, in terms of the framework of this paper.

The model of inhomogeneity of the current employed here was one-dimensional. Further generalizations of theory are needed if the current sheets are of limited extent in both transverse directions. Even within a one-dimensional model, there could be a sub-structure on a shorter distance scale, or even a random or stochastic current structure superposed on the underlying smooth current profile. These aspects also would require further generalizations. Thus it would be very valuable to learn from the present and future observations the detailed nature of the current distributions.

It is equally important to classify all the available observations on the ion cyclotron waves according to the satellite transit direction and study its correlations, if any, to the peak frequency and the width of the observed power spectrum.

Further improvements in understanding the CDICI can come in a number of other ways as well. Additional generalizations of theory should include variation (i.e., inhomogeneities) along the field lines. In terms of applications of the theory of the present level one should certainly consider multi-species plasmas, wider ranges of the ion to electron temperature ratio τ, wider ranges of the driving current V_d^o/v_e, and effects on higher harmonics. In terms of interpretation the results can be recast in terms of the convective growth rate approach (Ashour-Abdalla and Thorne, 1978), which takes into account the small group velocity of the ion cyclotron waves. These and other related topics are under further investigation.

We also note that Hwang, Fontheim and Ong (1983) have recently considered the effects on electrostatic waves of a cold electron current sheet of finite thickness, and concluded that the current sheet partially stabilizes the system and contributes to the coherence of the excited waves. Since they did not consider the effects of magnetic shear, the correspondence is with our regime (3), where the non-local effects stem directly from the finite width of the current channel. Even in this regime their approach is restricted to $\rho_i \ll L_c$. Also their assumption of a sharp change in the current at the boundaries is not pertinent to the space plasmas. We also note that they have concentrated more on the ion-acoustic wave, and have no thermal spreads, but some of their conclusions are similar to ours.

ACKNOWLEDGMENTS

We would like to thank Dr. Joel Fedder of the Naval Research Laboratory for numerous useful comments. We also wish to thank Dr. M. Temerin and Dr. D. Winningham for very helpful discussions regarding space plasma observational data and procedures, past and present. This work was supported by the Office of the Naval Research and the National Aeronautics and Space Administration.

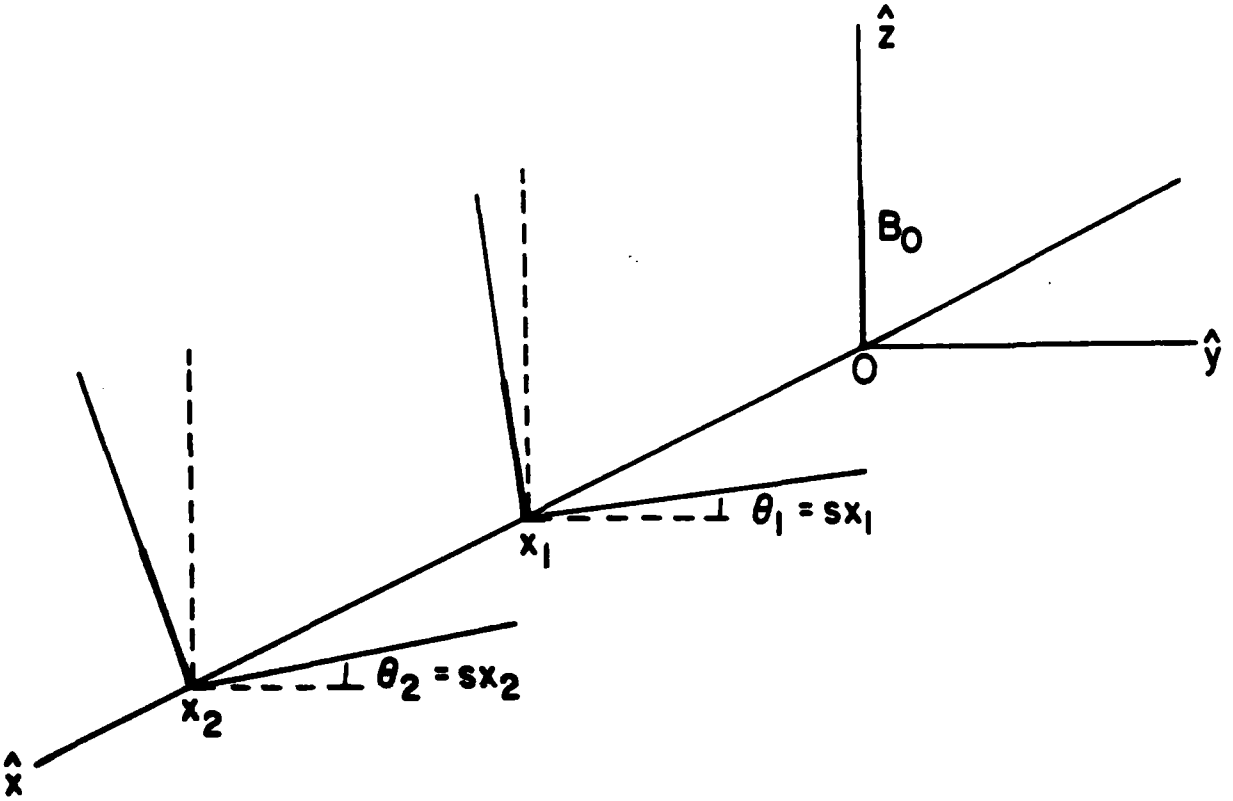

Figure 1. A sketch of a sheared magnetic field. At $x = 0$ the magnetic field B_0 is in the 2-direction. At $x = x_1$ the magnetic field rotates by an angle $\theta_1 = sx_1$, where $s = 1/L_s$. A wave perpendicular to the magnetic field B_0 at $x = 0$ is no longer so at $x = x_1$.

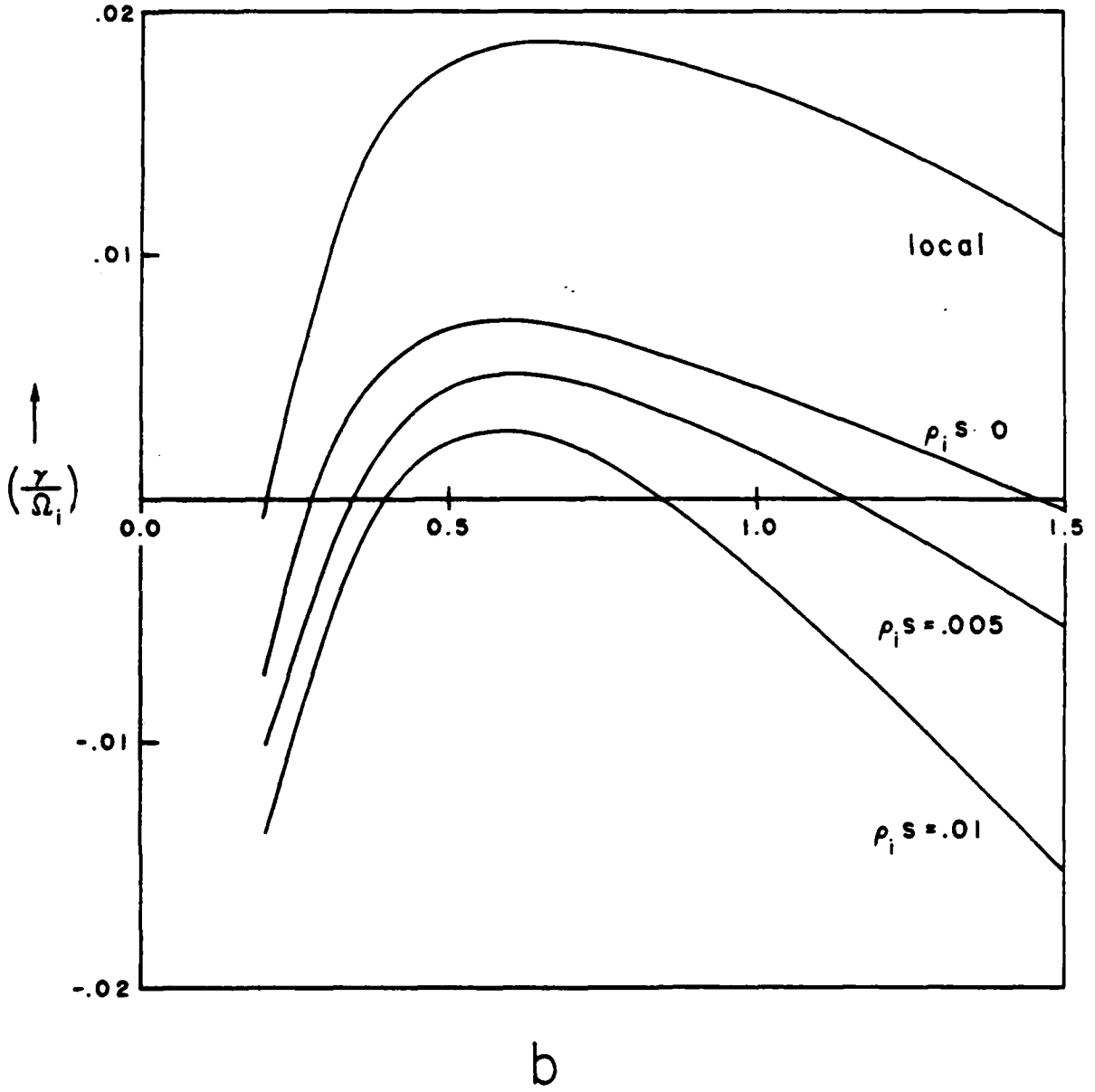

Figure 2. A plot of the growth rate (γ/Ω_i) against b for various shear values. Here $\tau = 0.5$, $\mu = 1837$, and $V_d/v_e = 0.25$. The big difference between the local solution and the $(\rho_i s) = 0$ limit of the non-local solution is due to a shear independent term arising from the non-local treatment. The curves also indicate that the effect of the shear is more pronounced for larger b.

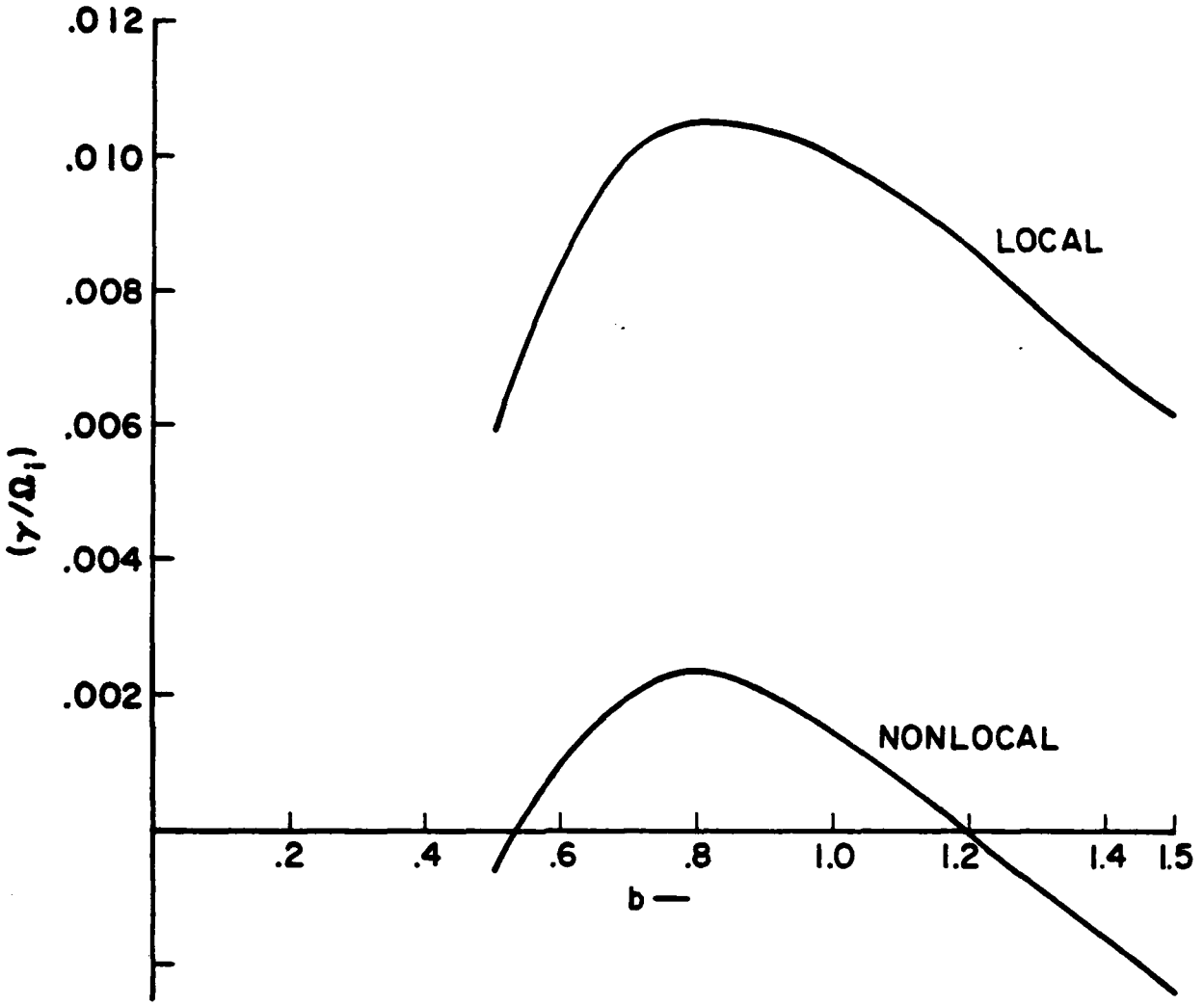

Figure 3. A plot similiar to Figure 2. Here $\tau = 0.75$, $\mu = 1837$ and $V_d/v_e = 0.3$. We provide only the local and the non-local spectrum. The non-local curve has a very small shear, $(\rho_i s) = 10^{-6}$. Note the significant reduction in the unstable perpendicular wavevector band.

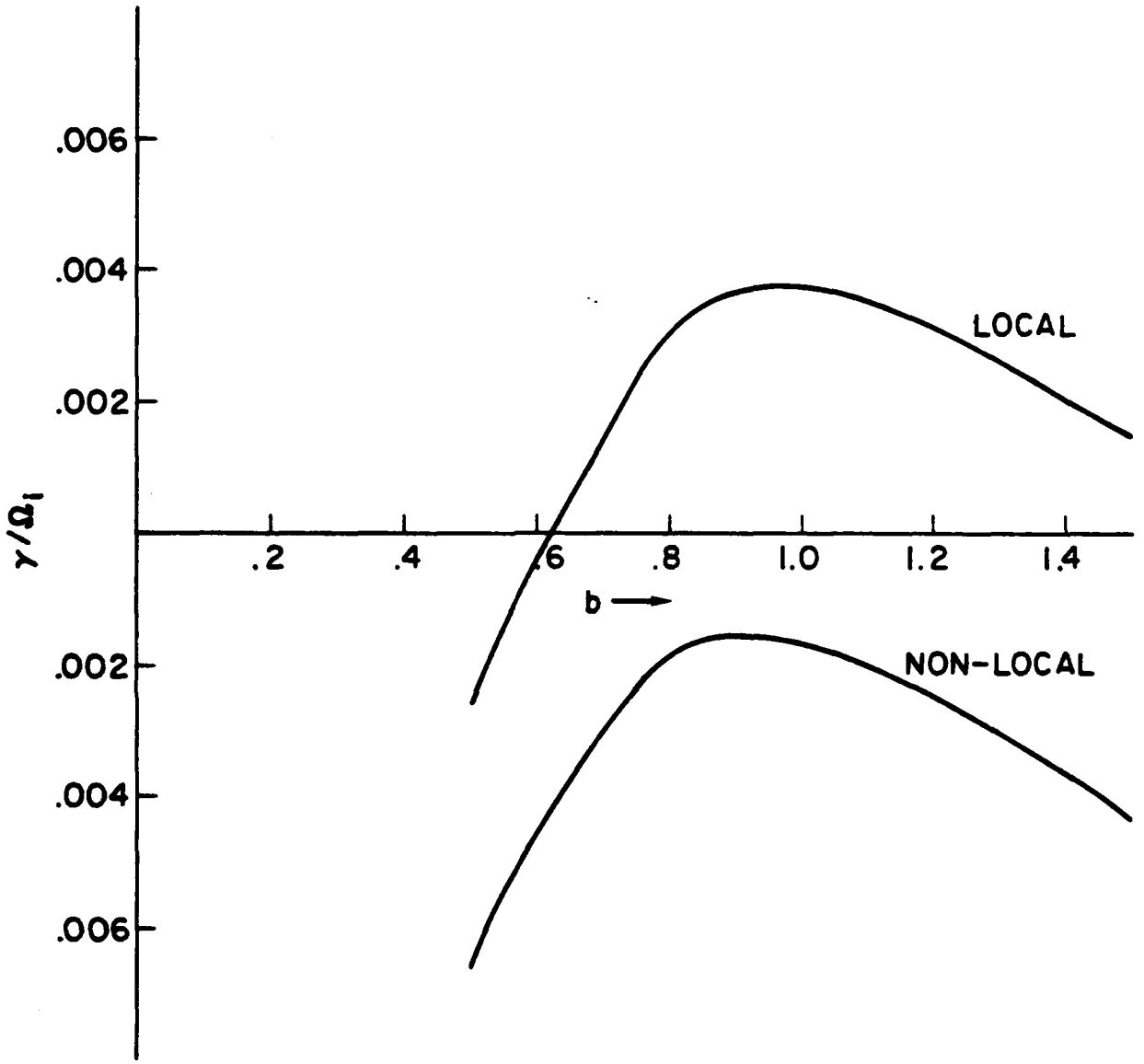

Figure 4. Growth rate versus b plot for $\mu = 1837$, and $V_d/v_e = 0.35$. The effect of the non-local treatment is very drastic in this case. The instability is totally suppressed.

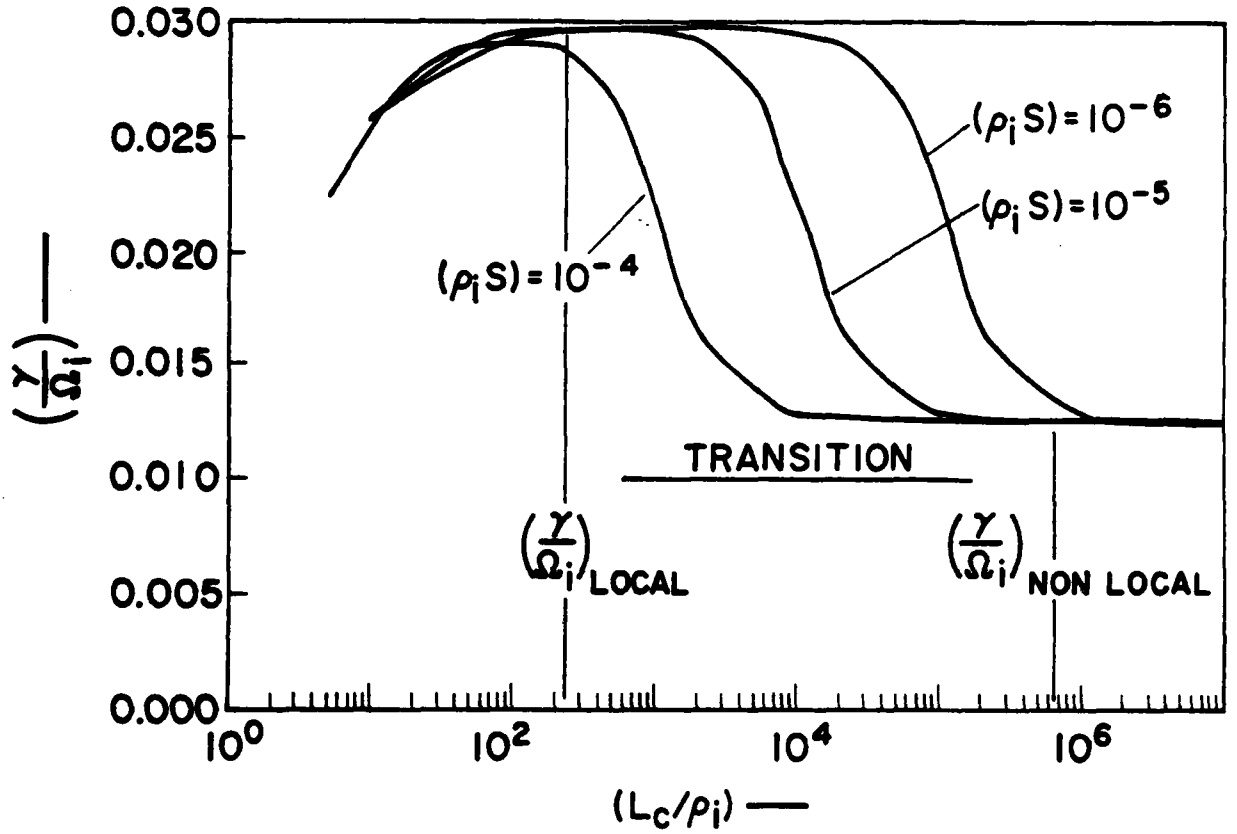

Figure 5. A plot of the growth rate $\left(\frac{\gamma}{\Omega_i}\right)$ against the current channel width (L_c/ρ_i) for three different magnetic shear lengths. Here $V_d^o = 0.28\ v_e$, $\mu = 1837$, $b = 0.6$, and $\tau = 0.5$.

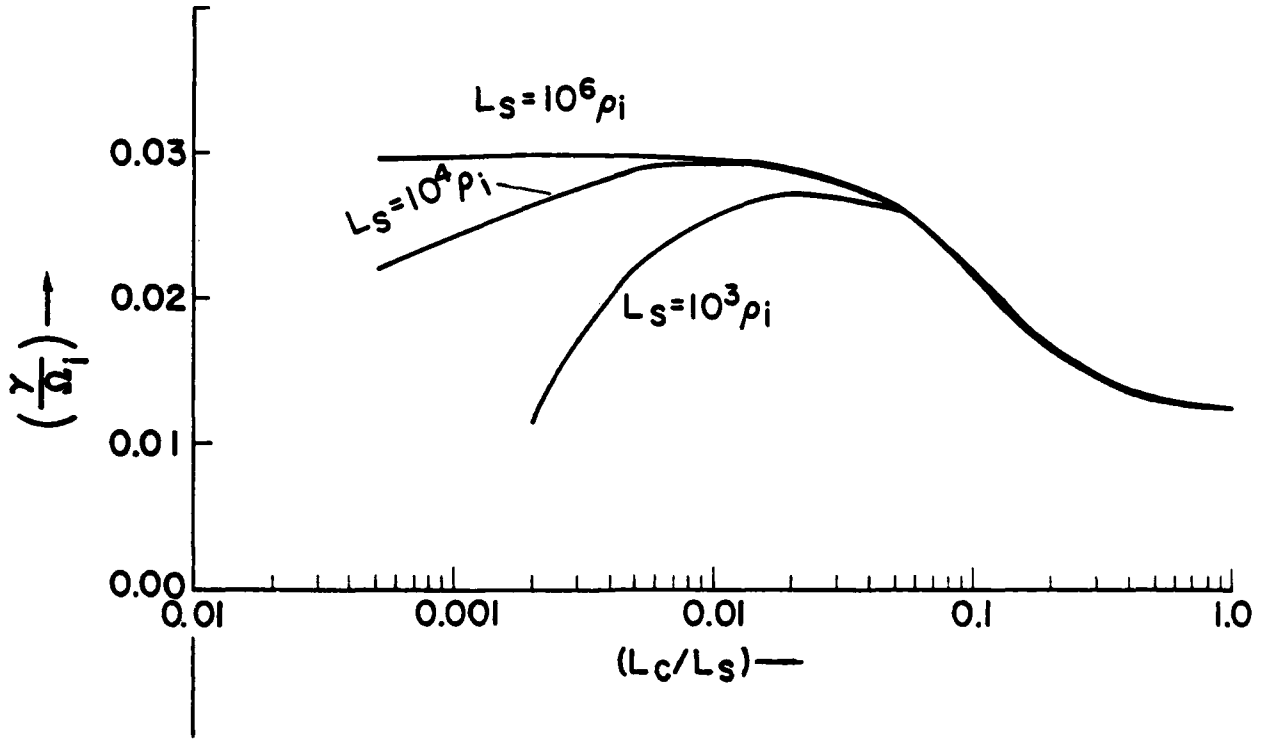

Figure 6. A plot of (γ/Ω_i) against (L_c/L_s) for three different L_s values. Here $b = 0.6$, $\mu = 1837$, $\tau = 0.5$, and $V_d^o = 0.28\ v_e$. The transition from local to the nonlocal results are universal, almost independent of the shear value.

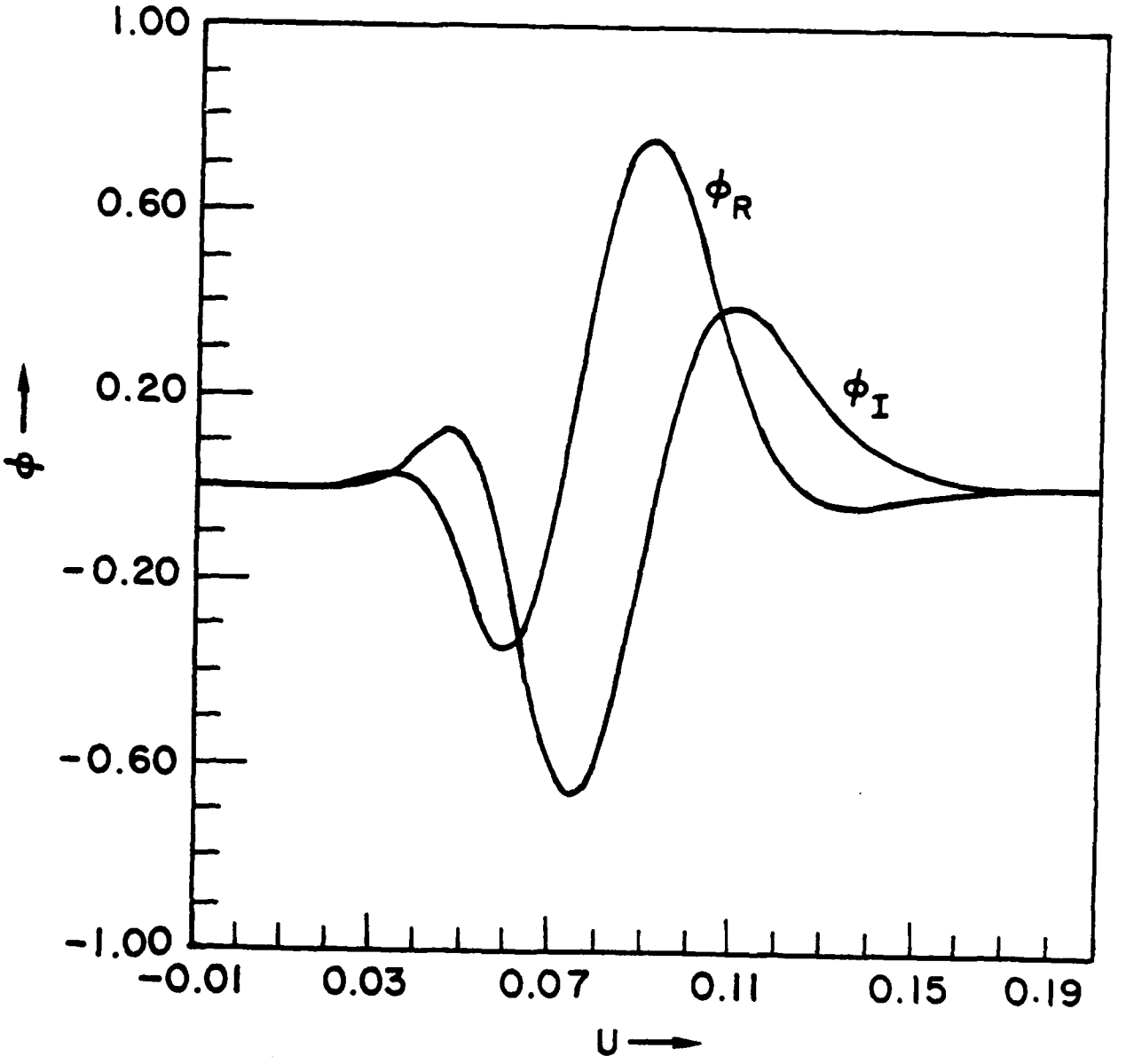

Figure 7. A plot of $\phi(u)$ against u for $L_c/\rho_i = \infty$, and $(\rho_i s) = 10^{-2}$, b = 0.6, $V_d^o = 0.28\ v_e$, and $\tau = 0.5$.

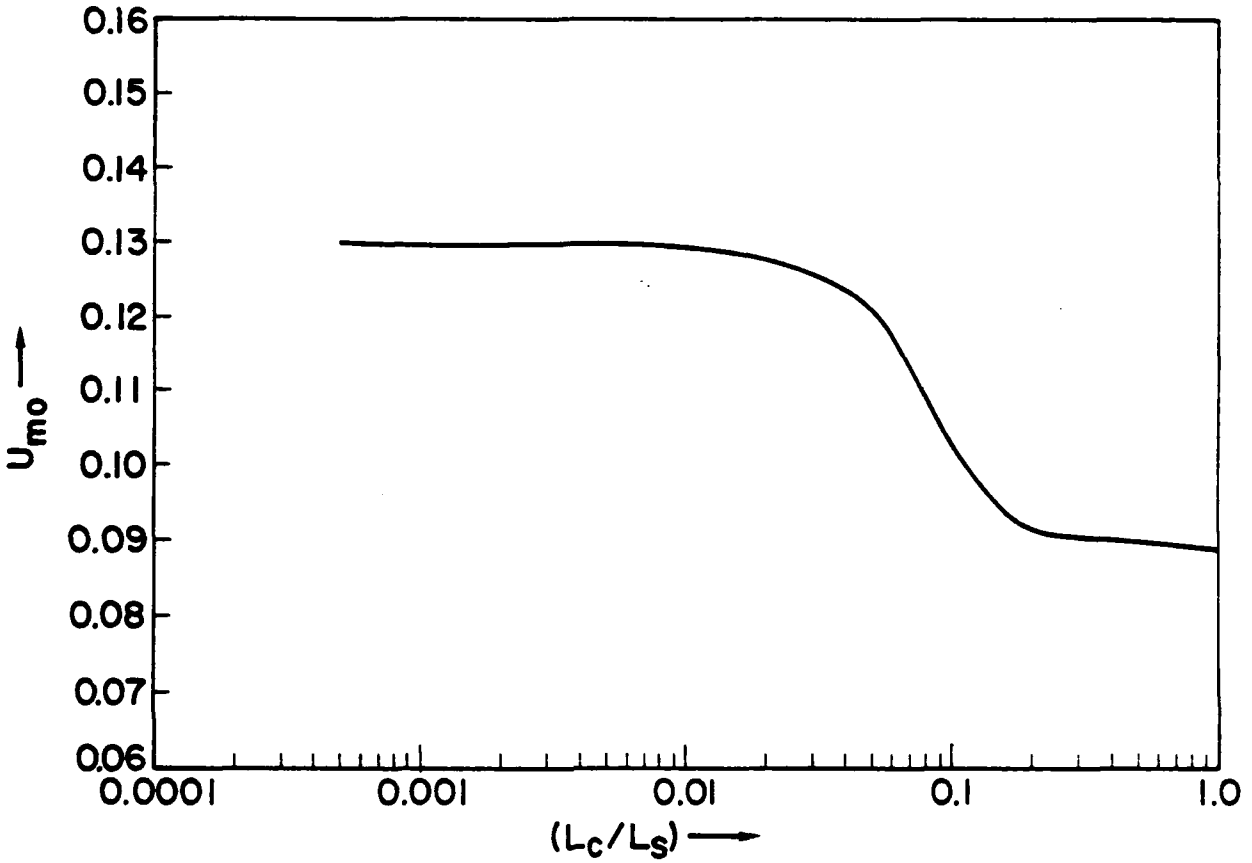

Figure 8. A plot for the real angle U_{mo} where $|\phi(u)|$ attains its maximum, against L_c/L_s. The physical parameters are same as in Figure 6.

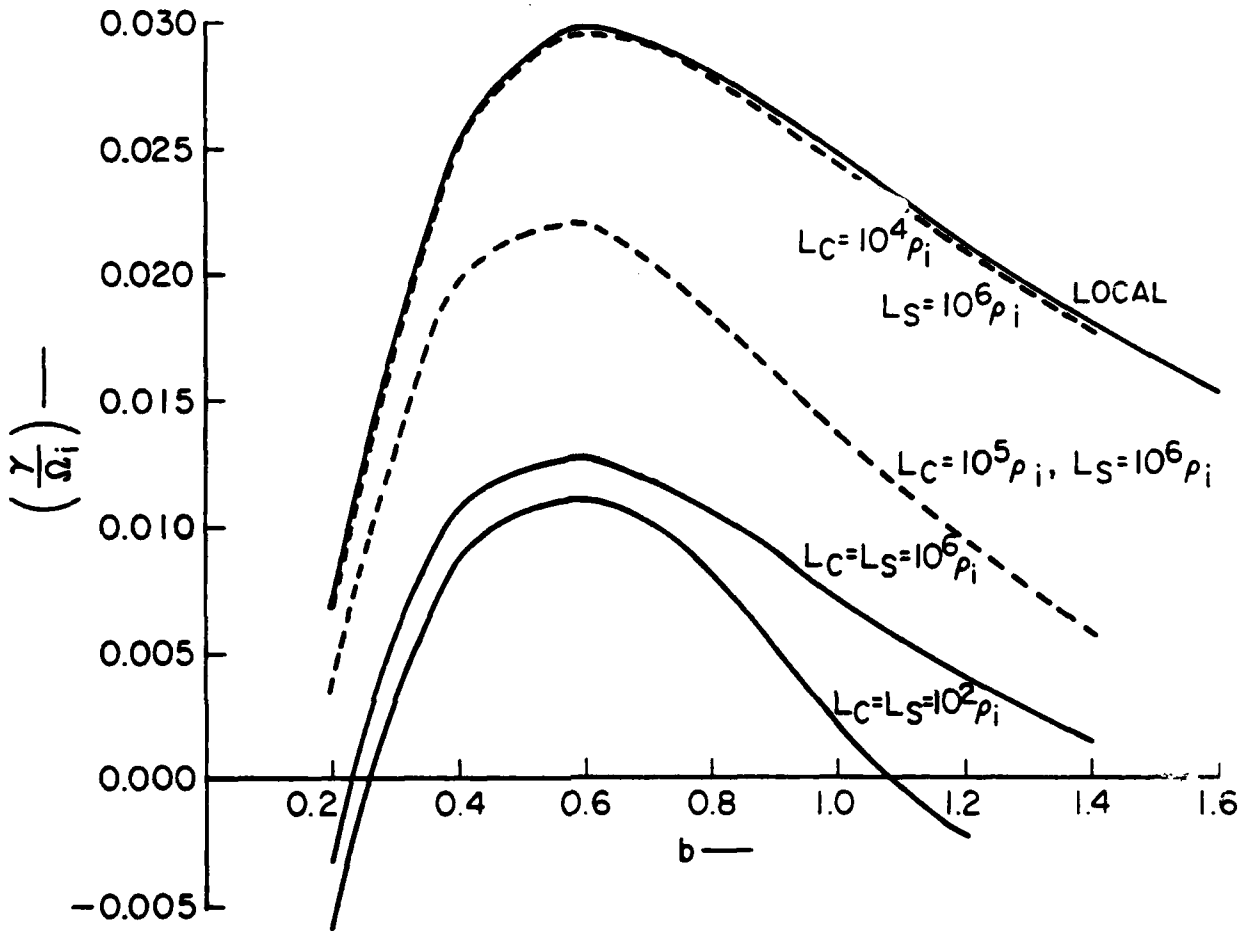

Figure 9. A plot of the growth rates against b. Here $\tau = 0.5$, $\mu = 1837$, $V_d^o = 0.28\ v_e$. The dotted lines show the transition from local to nonlocal values as L_c approaches L_s. The lowest solid line is for $L_c = L_s = 10^2 \rho_i$.

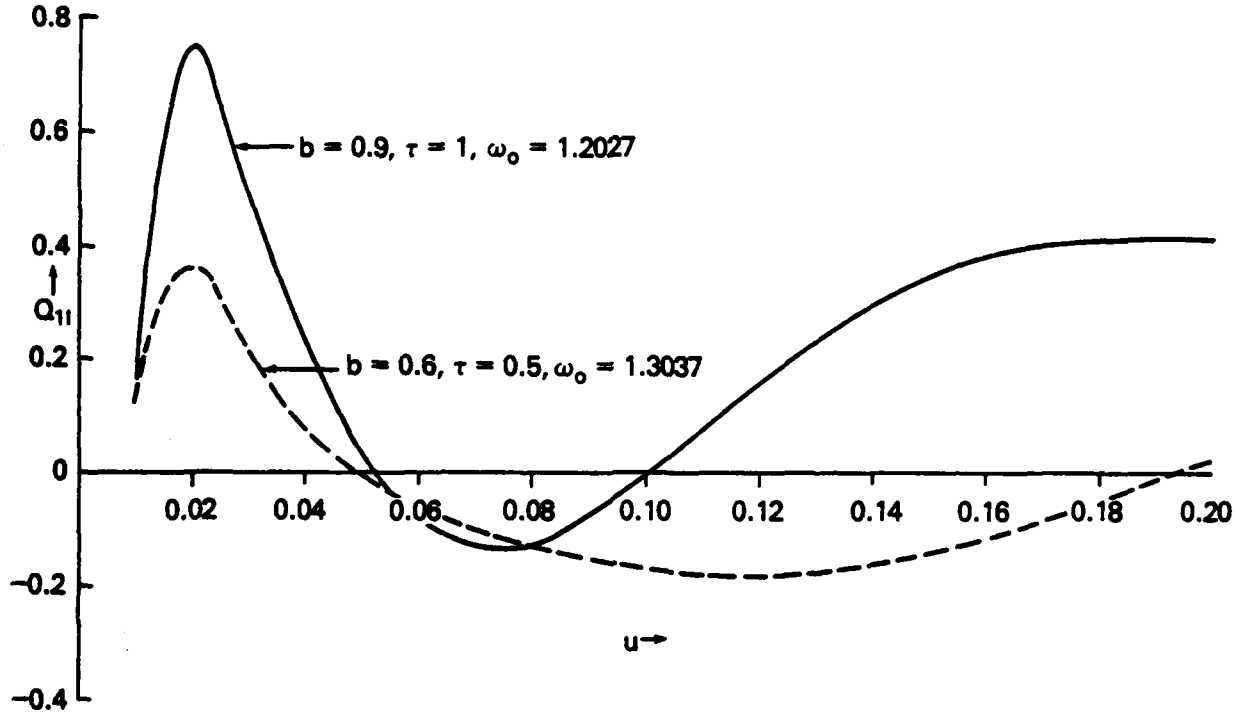

Figure 10. A plot of Q_{1I} vs. u for τ = 0.5 and 1, maximized over b to attain maximal growth rates.

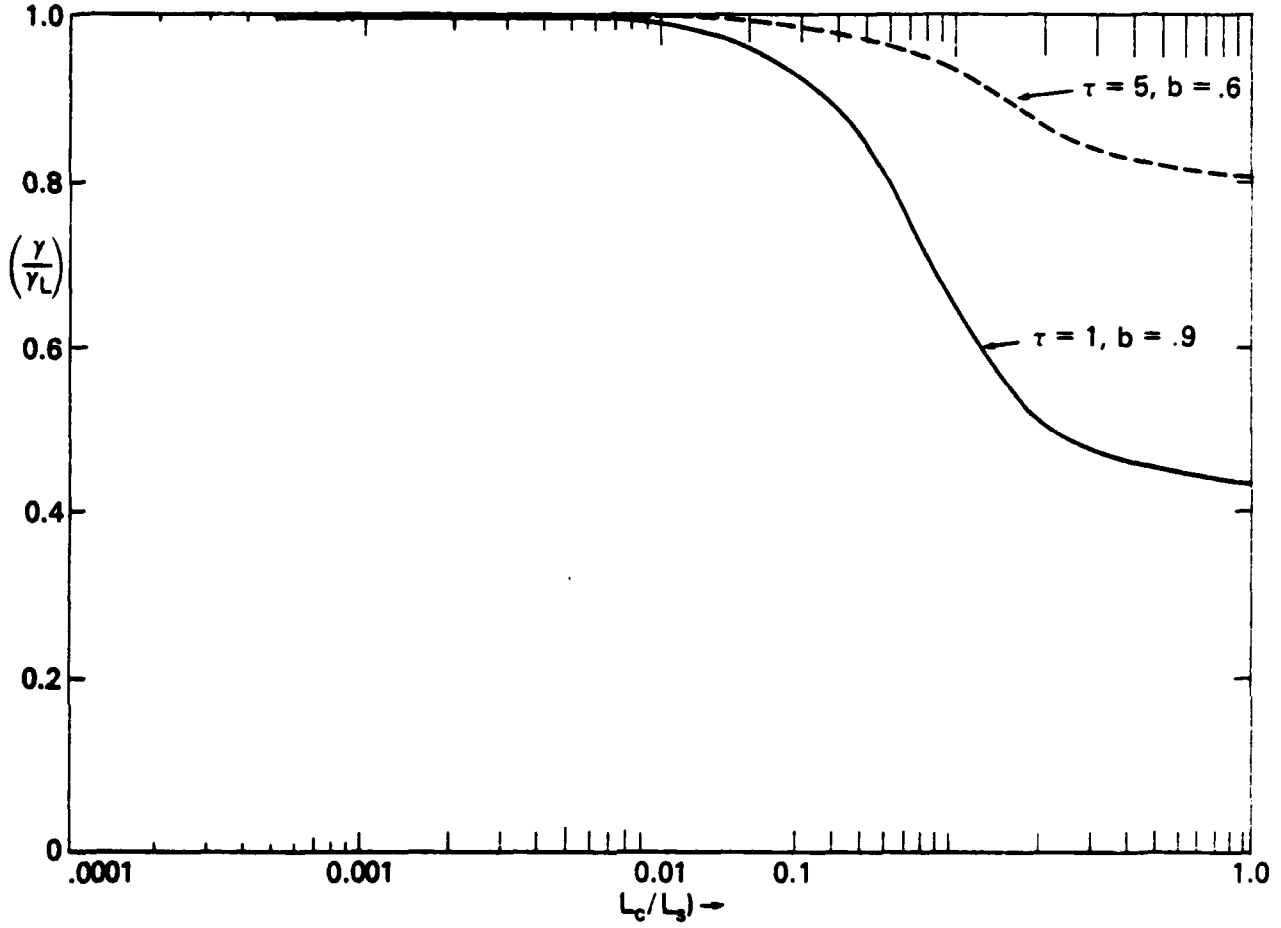

Figure 11. A plot of γ/γ_L vs. L_c/L_s for τ = 0.5 and 1, for the parameters of Figure 10.

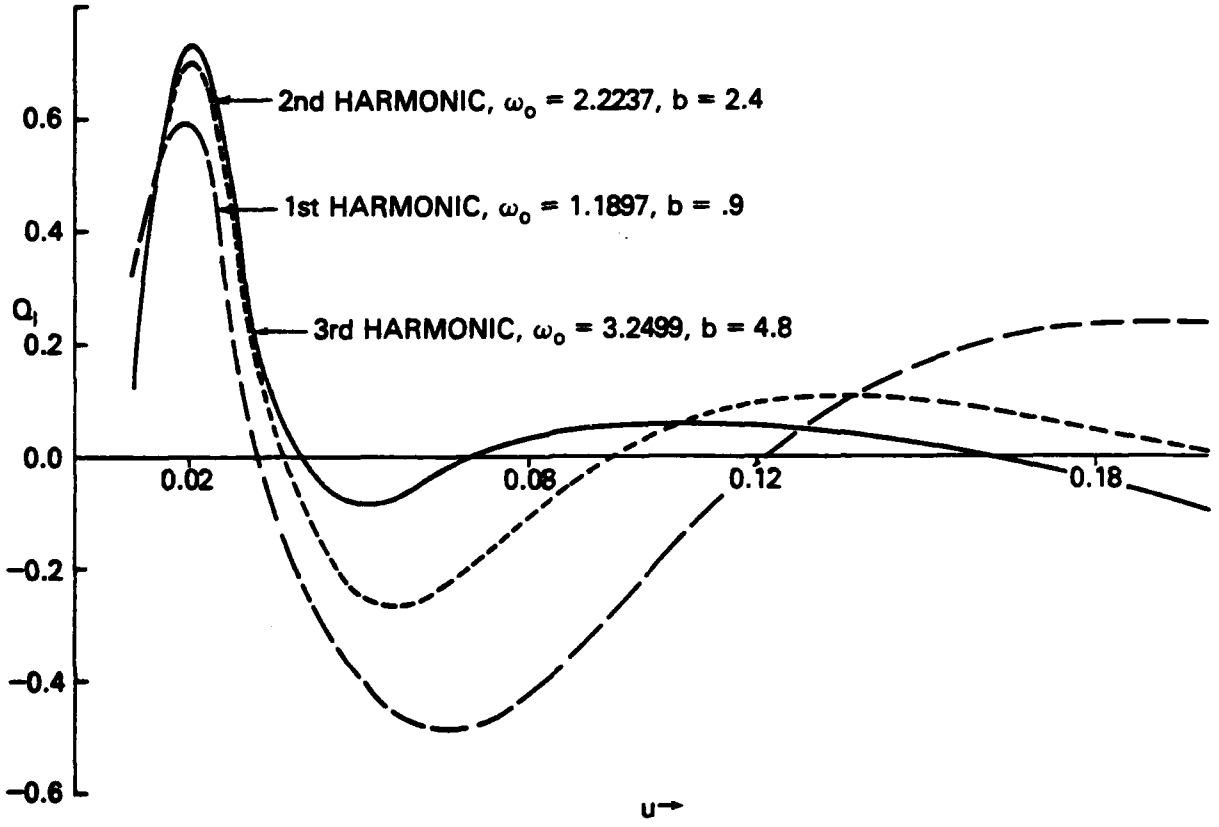

Figure 12. A plot of Q_{1I} vs. u for the first three cyclotron harmonics for $\tau = 1$, $V_d/v_e = 0.65$, maximized over b to attain maximal growth rates. The solid line is the third harmonic, the dashed line with small dashes is the second harmonic and the dashed line with the large dashes is the first harmonic.

REFERENCES

Ashour-Abdalla, M. and R.M. Thorne, Toward a Unified View of Diffuse Auroral Precipitation, J. Geophys. Res., 83, 4755, 1978.

Bakshi, P., W. Bellew, G. Ganguli, and P. Satyanarayana, Particle Orbits in Sheared Magnetic Fields and Drift Wave Instabilities, Abstract G1, Annual Controlled Fusion Theory Meeting, San Diego, 1977.

Bakshi, P., G. Ganguli, and P. Palmadesso, Finite Width Currents, Magnetic Shear and the Current Driven Ion Cyclotron Instability, Phys. Fluids, 26, 1808, 1983.

Bellew, W., Application of Operator Methods to an Inhomogeneous Plasma in a Sheared Magnetic Field, Ph.D Thesis, Boston College, 1978.

Drummond, W.E. and M.N. Rosenbluth, Anomalous Diffusion Arising from Microinstabilities in a Plasma, Phys. Fluids, 5, 1507, 1962.

Ganguli, G., Effects of Magnetic Shear on Ion-Cyclotron Modes, Ph.D Thesis, Boston College, 1980.

Ganguli, G. and P. Bakshi, Non-Local Aspects of Electrostatic Current Driven Ion Cyclotron Instability Due to Magnetic Shear, Phys. Fluids 25, 1830, 1982.

Hwang, K.S., E.G. Fontheim and R.S.B. Ong, Excitation of an Electrostatic Wave by a Cold Electron Current Sheet of Finite Thickness, Planet. Space Sci., 31, 285, 1983.

Kindel, J.M. and C.F. Kennel, Topside Current Instabilities, J. Geophys. Res., 76, 3055, 1971.

Kintner, P.M., M.C. Kelly and F.S. Mozer, Electrostatic Hydrogen Cyclotron Waves Near One Earth Radius Altitude in the Polar Magnetosphere, Geophys. Res. Lett., 5, 139, 1978.

Kintner, P.M., On the Distinction Between Electrostatic Ion Cyclotron Waves and Ion Cyclotron Harmonic Waves, Geophys. Res. Lett., 7, 585, 1980.

Linsker, R., Integral-Equation Formulation for Drift Eigen Modes in Cylindrically Symmetric Systems, Phys. Fluids, 24, 1485, 1981.

Pearlstein, L.D. and H.L. Berk, Universal Eigen Mode in a Strongly Sheared Magnetic Field, Phys. Rev. Lett., 23, 220, 1969.

Ross, D W. and S.M. Mahajan, Are Drift-Wave Eigen Modes Unstable?, Phy. Rev. Lett., 40, 324, 1978.

TFR Group, Ion-Cyclotron Instability in the TFR Tokamak, Phys. Rev. Lett., 41, 113, 1978.

Waltz, R.E. and R.R. Dominguez, Ion Cyclotron Modes in Tokamaks, Phys. Fluids, 24, 1575, 1981.

DISTRIBUTION LIST

Director
Naval Research Laboratory
Washington, D.C. 20375
ATTN: Code 4700 (26 Copies)
Code 4701
Code 4780 (100 copies)
Code 4187 (E. Szuszczewicz)
Code 4187 (P. Rodriguez)
Code 2628 (22 copies)

University of Alaska
Geophysical Institute
Fairbanks, Alaska 99701
ATTN: Library
S. Akasofu
J. Kan
J. Roederer
L. Lee

University of Arizona
Dept. of Planetary Sciences
Tucson, Arizona 85721
ATTN: J.R. Jokipii

University of California, S.D.
LaJolla, California 92037
(Physics Dept.):
ATTN: J.A. Fejer
T. O'Neil
J. Winfrey
Library
J. Malmberg
(Dept. of Applied Sciences):
ATTN: H. Booker

University of California
Los Angeles, California 90024
(Physic Dept.):
ATTN: J.M. Dawson
B. Fried
J.G. Moralles
W. Gekelman
R. Stenzel
Y. Lee
A. Wong
F. Chen
M. Ashour-Abdalla
Library
J.M. Cornwall

(Institute of Geophysics and
Planetary Physics):
ATTN: Library
C. Kennel
F. Coroniti

Columbia University
New York, New York 10027
ATTN: R. Taussig
R.A. Gross

University of California
Berkeley, California 94720
(Space Sciences Laboratory):
ATTN: Library
M. Hudson
(Physics Dept.):
ATTN: Library
A. Kaufman
C. McKee
(Electrical Engineering Dept.):
ATTN: C.K. Birdsall

University of California
Physics Department
Irvine, California 92664
ATTN: Library
G. Benford
N. Rostoker
C. Robertson
N. Rynn

California Institute of Technology
Pasadena, California 91109
ATTN: R. Gould
L. Davis, Jr.
P. Coleman

University of Chicago
Encrico Fermi Institute
Chicago, Illinois 60637
ATTN: E.N. Parker
I. Lerche
Library

University of Colorado
Dept. of Astro-Geophysics
Boulder, Colorado 80302
ATTN: M. Goldman
Library

Cornell University
School of Applied and Engineering Physics
College of Engineering
Ithaca, New York 14853
ATTN: Library
R. Sudan
B. Kusse
H. Fleischmann
C. Wharton
F. Morse
R. Lovelace

Harvard University
Cambridge, Massachusetts 02138
ATTN: Harvard College Observatory
(Library)
G.S. Vaina
M. Rosenberg

Harvard University
Center for Astrophysics
60 Garden Street
Cambridge, Massachusetts 02138
ATTN: G.B. Field

University of Iowa
Iowa City, Iowa 52240
ATTN: C.K. Goertz
D. Garnett
G. Knorr
D. Nicholson

University of Houston
Houston, Texas 77004
ATTN: Library

University of Maryland
Physics Dept.
College Park, Maryland 20742
ATTN: K. Papadopoulos
H. Rowland
C. Wu

University of Michigan
Ann Arbor, Michigan 48140
ATTN: E. Fontheim

University of Minnesota
School of Physics
Minneapolis, Minnesota 55455
ATTN: Library
J.R. Winckler
P. Kellogg

M.I.T.
Cambridge, Massachusetts 02139
ATTN: Library
(Physics Dept.):
ATTN: B. Coppi
V. George
G. Bekefi
T. Dupree
R. Davidson
(Elect. Engineering Dept.):
ATTN: R. Parker
A. Bers
L. Smullin
(R.L.E.):
ATTN: Library
(Space Science):
ATTN: Reading Room

Princeton University
Princeton, New Jersey 08540
Attn: Physics Library
Plasma Physics Lab. Library
C. Oberman
F. Perkins
T.K. Chu
H. Okuda
V. Aranasalan
H. Hendel
R. White
R. Kurlsrud
H. Furth
S. Yoshikawa
P. Rutherford

Rice University
Houston, Texas 77001
Attn: Space Science Library
R. Wolf

University of Rochester
Rochester, New York 14627
ATTN: A. Simon

Stanford University
Institute for Plasma Research
Stanford, California 94305
ATTN: Library

Stevens Institute of Technology
Hoboken, New Jersey 07030
ATTN: B. Rosen
G. Schmidt
M. Seidl

University of Texas
Austin, Texas 78712
ATTN: W. Drummond
V. Wong
D. Ross
W. Horton
D. Choi
R. Richardson
G. Leifeste

College of William and Mary
Williamsburg, Virginia 23185
Attn: F. Crownfield

Lawrence Livermore Laboratory
University of California
Livermore, California 94551
ATTN: Library
B. Kruer
J. Thomson
J. Nucholls
J. DeGroot
L. Wood
J. Emmett
B. Lasinsky
B. Langdon
R. Briggs
D. Pearlstein

Los Alamos National Laboratory
P.O. Box 1663
Los Alamos, New Mexico 87545
ATTN: Library
D. Forslund
J. Kindel
B. Bezzerides
H. Dreicer
J. Ingraham
R. Boyer
C. Nielson
K. Lindman
L. Thode

N.O.A.A.
325 Broadway S.
Boulder, Colorado 80302
ATTN: J. Weinstock
Thomas Moore (SEL, R-43)
W. Bernstein
D. Williams

Sandia Laboratories
Albuquerque, New Mexico 87115
ATTN: A. Toepfer
G. Yeonas
D. VanDevender
J. Freeman
T. Wright

Bell Laboratories
Murray Hill, New Jersey 07974
ATTN: A. Hasegawa

Lockheed Research Laboratory
Palo Alto, California 94304
ATTN: M. Walt
J. Cladis

Physics International Co.
2400 Merced Street
San Leandro, California 94577
ATTN: J. Benford
S. Putnam
S. Stalings
T. Young

Science Applications, Inc.
Lab. of Applied Plasma Studeis
P.O. Box 2351
LaJolla, California 92037
ATTN: L. Linson
J. McBride

Goddard Space Flight Center
Greenbelt, Maryland 20771
ATTN: M. Goldstein
T. Northrop
T. Birmingham

TRW Space and Technology Group
Space Science Dept.
Building R-1, Room 1170
One Space Park
Redondo Beach, California 90278
ATTN: R. Fredericks
W.L. Taylor

National Science Foundation
Atmospheric Research Section (ST)
Washington, D.C. 20550
ATTN: D. Peacock

Goddard Space Flight Center
Code 620
Greenbelt, Maryland 20771
ATTN: Robert F. Benson

NASA Headquarters
Code EE-8
Washington, D.C. 20546
ATTN: Dr. I. Schmerling
Dr. J. Lynch
Dr. D. Butler

Klumpar, David
Center for Space Sciences
P.O. Box 688
University of Texas
Richardson, Texas 75080

Leung, Philip
Dept. of Physics
University of California
405 Hilgard Avenue
Los Angeles, California 90024

Lysak, Robert
School of Physics and Astronomy
University of Minnesota
Minneapolis, MN 55455

Schulz, Michael
Aerospace Corp.
A6/2451, P.O. Box 92957
Los Angeles, California 90009

Shawhan, Stanley
Dept. of Physics & Astronomy
University of Iowa
Iowa City, Iowa 52242

Temerin, Michael
Space Science Lab.
University of California
Berkeley, California 94720

Vlahos, Loukas
Dept. of Physics
University of Maryland
College Park, Maryland 20742

Matthews, David
IPST
University of Maryland
College Park, Maryland 20742

Schunk, Robert W.
Utah State University
Dept. of Physics
Logan, Utah 84322

END

FILMED

11-83

DTIC